

Research Article

E-Gear Functionality Based on Mechanical Relays in Permanent Magnet Synchronous Machines

Lynn Verkroost^{1,2}, **Mauro Demeyer**¹, **Homayoun Soltani Gohari**^{1,2}, **Johan Lecoutere**³, **Peter Sergeant**^{1,2} and **Hendrik Vansompel**^{1,2}

¹Electrical Energy Laboratory, Department of ElectroMechanical, Systems and Metal Engineering, Ghent University, Ghent 9000, Belgium

²Flanders Make@UGent—MIRO, Ghent, Belgium

³Bluways International bv, Leuven 3001, Belgium

Correspondence should be addressed to Lynn Verkroost; lynn.verkroost@ugent.be

Received 22 February 2024; Revised 7 August 2024; Accepted 28 August 2024

Academic Editor: Jagabar Sathik

Copyright © 2024 Lynn Verkroost et al. This is an open access article distributed under the Creative Commons Attribution License, which permits unrestricted use, distribution, and reproduction in any medium, provided the original work is properly cited.

Permanent magnet synchronous machines (PMSMs) are still the first choice for use in electric vehicles, due to their unparalleled efficiency and power density. However, they suffer from an inherently limited speed range. As field weakening or the addition of a mechanical gearbox deteriorates the efficiency of the drive, it is suggested in this paper to equip the drive with reconfiguration switches, giving rise to a so-called e-gear. The switches—which are implemented by means of mechanical relays—allow to change the winding connection of the electric machine from a series to a parallel connection and hence to double its efficient speed range. Simulations and experimental results on a 4-kW axial-flux PMSM confirm the feasibility of the concept and prove that the reconfiguration can be conducted in less than 35 ms.

1. Introduction

The key drivers for electric motor development for electric vehicles nowadays are compactness, power density, energy efficiency, and cost. As a result, permanent magnet synchronous machines (PMSMs) with NdFeB magnets are still commonly used for electric traction applications, due to their unmatched efficiency, power density, and torque density [1, 2]. However, as the back electromotive force (EMF) of PMSMs is proportional to their speed, the available DC bus voltage limits their speed.

One solution to deal with this restricted speed range is field weakening. A d -axis current is injected in the PMSM, in order to reduce the flux linkage—and hence the back EMF—originating from the permanent magnets. Field weakening only requires an adaptation of the control strategy and is thus easy to implement. However, the achievable speed range extension is limited by the motor design, the DC bus voltage, and the voltage rating and current rating of the inverter. Furthermore, the injection of the d -axis current comes at

the cost of the motor's efficiency, its torque output, and its dynamic performance [3, 4].

Other state-of-the-art solutions to deal with the quite narrow efficient speed range of a PMSM are the addition of a mechanical gearbox or the addition of a buck–boost DC–DC converter. Pulse amplitude modulation (PAM) control with such a buck–boost DC–DC converter not only allows to boost the DC-link voltage in order to achieve higher speeds but also reduces the voltage distortion at low speeds [5, 6, 7]. However, both a gearbox and a buck–boost converter cause additional complexity and losses.

The fact that electric motors with a fixed winding configuration only have a limited operating range can also be circumvented by so-called winding changeover techniques. These reconfiguration strategies make use of the fact that each specific connection between the windings of an electric machine results in its own specific operating range and efficiency map. Reconfiguration switches make it possible to switch between different winding connections and hence to extend the efficient operating range of the electric motor [8].

In this way, a so-called e-gear can be established: an electric machine that can shift its winding connection, depending on its operating point. The switching unit can be simultaneously designed with the electric machine, or it can be retrofitted. It does not alter the rated power or maximum torque of the electric machine.

A multitude of winding changeover techniques or reconfiguration strategies already exist in literature. Two main categories can be discerned, based on the type of switches: e-gears with semiconductor-based switches (e.g., thyristors, insulated-gate bipolar transistor [IGBTs], and triode for alternating current [TRIACs]) or e-gears with mechanical switches (e.g., relays and contactors). The use of semiconductor-based switches has the advantage that the transition time to switch from one configuration to the other is very short (in the order of a few microseconds) and that the predicted lifetime of semiconductor-based switches in an electrical vehicle amounts to at least a couple of years under the New York city cycle (NYCC) [9]. However, due to the fact that the current that needs to be redirected by the reconfiguration strategies is an AC current, bulky, expensive, and often bidirectional switching units are required, with an undesirably high number of semiconductor-based switches and their accompanying conduction losses [8]. Mechanical switches, on the other hand, can realise the same changes in winding connection in a simpler and less expensive way and do not suffer from the same level of conduction losses. On the other hand, mechanical switches exhibit transition times in the order of tens to hundreds of milliseconds due to mechanical constraints, and they are prone to wear [3]. However, even the most advanced mechanical gearboxes in cars exhibit shift times in the same order of magnitude [10]. Furthermore, as the mechanical lifetime of mechanical relays is expected to be at least one million operations [11], also the lifetime of the relays is not a real restriction for electric passenger vehicles, which are only designed for less than 500,000 km themselves [1].

A well-known example of a winding changeover is the wye-delta reconfiguration. The wye configuration covers the high torque/low speed range, while the delta configuration covers the low torque/high speed range. This reconfiguration can be implemented using six mechanical contactors [12] or using at least eight IGBTs, diodes, and gate drivers [3]. Sadeghi et al. [13] extended the concept to five-phase machines, which can switch between a star, a pentagon, or a pentacle configuration.

Another way to reduce the back EMF of a PMSM is to reduce its number of stator turns. A tap-changer circuit allows to feed only part of a wye-connected phase winding. Multiple implementations can be found in the literature. Kume et al. [14], for instance, used mechanical contactors. The tap-changer circuit in [3, 15, 16], on the other hand, consists of two three-phase diode bridges, two IGBT switches, a snubber circuit, and two precharge resistors. The use of the snubber circuit and its corresponding losses are avoided in [17] by using a circuit made of six semiconductor switches and diodes. However, a main disadvantage of this tap-changing technique is the low utilisation rate of the motor windings, as

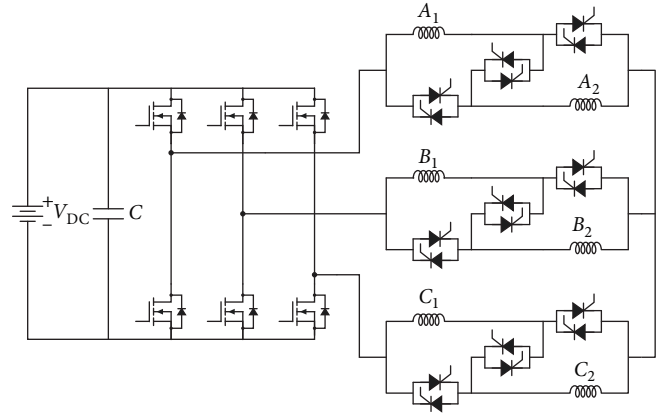


FIGURE 1: Series/parallel reconfiguration by means of nine thyristors [16].

only part of the motor windings is used in high-speed mode [14].

This low utilisation rate of the motor windings is not an issue when using a series/parallel reconfiguration. High torque levels can be achieved with the series connection, while the parallel connection allows to extend the speed range. This reconfiguration is accomplished in [16] by means of nine thyristors, with a reported loss of 1,296 W in the reconfiguration unit of a 80 kW drive. This semiconductor-based e-gear is shown in Figure 1. The high conduction losses in the thyristors can be avoided by using mechanical switches instead of semiconductor-based switches. The implementation of the series/parallel reconfiguration with six mechanical switches as shown in Figure 2 is conceptualised in [17] but to the authors' best knowledge has not yet been further developed in the literature.

As the disadvantages of mechanical relays (i.e., their finite transition time and limited lifetime) are no deal breakers for electric vehicles, the goal of this paper is therefore to elaborate on the PMSM e-gear with mechanical switches depicted in Figure 2. This e-gear requires three single pole single throw power relays and three single pole double throw power relays to switch between a series and a parallel connection. Its physical implementation is discussed in Section 2. The extension of the operating range and the efficiency of the drive are studied in Section 3. The reconfiguration switching itself and its transition time are the subjects of Section 4.

2. E-Gear Architecture and Experimental Test Setup

The series/parallel e-gear depicted in Figure 2 can be code-signed as a single unit, or the reconfiguration unit can be retrofitted on a standard PMSM with a standard three-phase drive. The only requirements for the PMSM are that it has two paths per phase with identical back EMF and that it has open-end windings. If the back EMF of the parallel paths is not identical in amplitude or in phase, circulating currents occur in the parallel mode, which deteriorate the efficiency or even exceed the current limits of the PMSM. The series/parallel

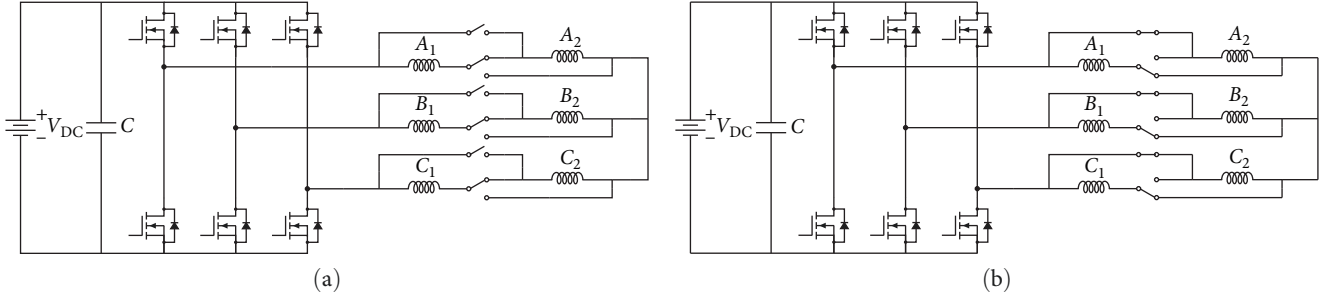


FIGURE 2: Series/parallel reconfiguration by means of three single pole single throw power relays and three single pole double throw power relays: (a) series connection and (b) parallel connection.



FIGURE 3: Stator tooth with bifilar winding.

reconfiguration can be applied to both concentrated and distributed winding configurations.

Depending on the initial motor design, the required parallel paths can be automatically present in the PMSM. A PMSM with 48 stator slots and four pole pairs, for instance, inherently has four parallel paths with identical back EMF per phase. Another option to create the parallel paths is the use of a bifilar winding, as shown in Figure 3. In this case, two parallel strands are wound together at the same time, making two contiguous windings. This last technique can be applied to any motor, regardless of its number of stator slots or stator teeth and its number of pole pairs.

In this paper, the series/parallel e-gear functionality is implemented on a 4-kW segmented armature torus axial-flux permanent magnet synchronous machine (AFPMSM) with 15 stator teeth and eight pole pairs, and the specifications are summarised in Table 1. The structure of the AFPMSM is illustrated in Figure 4. The back EMFs in the 15 concentrated windings are shifted with an electrical angle of $2\pi/15$ electrical radians between them, as illustrated in the voltage phasor graph of Figure 4(c). It is hence impossible to combine the 15 concentrated windings into two three-phase sets with identical back EMF. The two parallel paths are therefore obtained by winding the 15 stator teeth bifilarly, as shown in Figure 3. The 60 power terminals are all accessible, as shown in Figure 5.

The series/parallel reconfiguration unit can be composed of three single pole single throw power relays and three single

TABLE 1: Machine parameters.

Parameter	Symbol	Value
Rated torque (N•m)	T_n	13
Rated speed (r/min)	N_n	2,500
Rated current per winding (A)	I_n	5.5
Number of pole pairs	N_p	8
Number of stator teeth	Q_s	15
Number of turns per stator tooth	N_w	57×2
Outer diameter (mm)	D_o	148
Inner diameter (mm)	D_i	100
Axial length core element (mm)	h_{tot}	60
<i>Six-phase machine model</i>		
Stator resistance (Ω)	R_s	0.65
Self inductance (mH)	L_m	3.546
	M_1	-0.0904
Mutual inductances (mH)	M_2	3.351
	M_3	-0.0844
Flux linkage caused by magnets (Wb)	Ψ_m	0.106
<i>Series configuration</i>		
Stator inductance (mH)	$L_{d,s} \approx L_{q,s}$	14.14
Flux linkage caused by magnets (Wb)	$\Psi_{m,s}$	0.212
<i>Parallel configuration</i>		
Stator inductance (mH)	$L_{d,p} \approx L_{q,p}$	3.54
Flux linkage caused by magnets (Wb)	$\Psi_{m,p}$	0.106

pole double throw power relays. In the test setup of Figure 5, however, it is opted to use six identical single pole double throw Potter & Brumfield T9GS5L14-5 power relays with a contact current rating of 20 A. As the cost of one relay is in the order of only a few euros, the switching unit can indeed be realised in an inexpensive way by means of these six mechanical relays. The use of a dedicated relay with a single coil could reduce the cost even further in series production.

The 4-kW AFPMSM is fed by means of a standard three-phase two-level voltage source inverter (2L-VSI) making use of Wolfspeed C3M0075120D SiC MOSFETs and Infineon 1ED020112-F2 gate drivers. The DC bus voltage V_{DC} is equal to 400 V and provided by a 15-kW Delta Elektronik SM500-CP-90 bidirectional DC power supply. The DC-link capacitance C equals 1,000 μ F. The AFPMSM is working in motor-ing mode under torque control, while its mechanical speed is set by means of an induction machine that is mounted on the

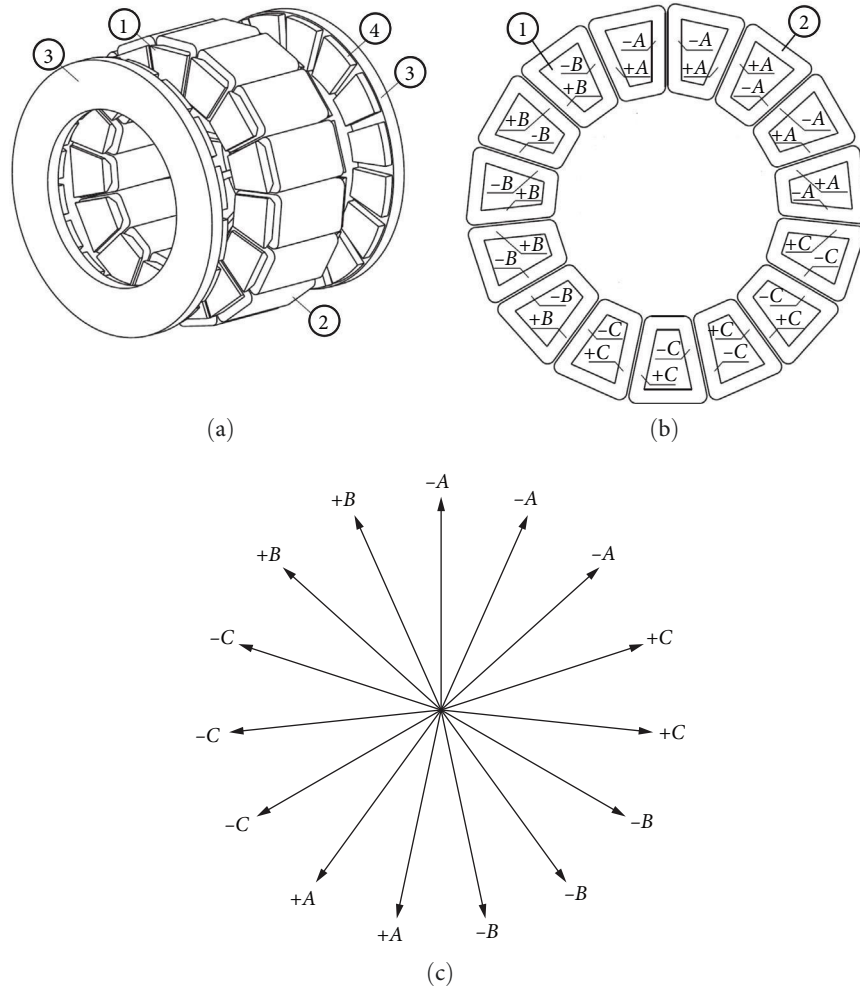


FIGURE 4: The AFPMSM consists of a stator comprising 15 stator core elements (1) with a bifilar tooth coil winding (2) and two rotor discs (3) with 16 permanent magnets per disc (4). Winding $X \in \{A, B, C\}$ represents a bifilar tooth coil winding comprising windings X_1 and X_2 : (a) 3D-view of the AFPMSM [18], (b) front view of the stator with winding arrangement [18], and (c) voltage phasor graph [18].

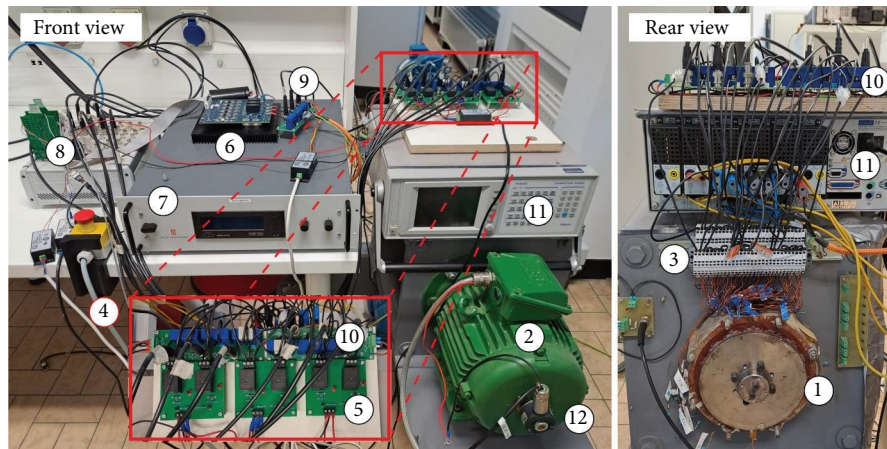


FIGURE 5: The test setup consists of an AFPMSM (1) and a load motor (2). The 60 power terminals (3) of the AFPMSM are accessible. The reconfiguration unit (4) consists of six mechanical relays (5). The AFPMSM is fed by means of a three-phase 2L-VSI (6) connected to a DC-source (7). The control is implemented on a dSPACE MicroLabBox (8). Current sensors provide feedback on the three-phase current fed by the inverter (9) and monitor the three-phase currents through the parallel paths (10). A power analyser (11) is used for electrical power measurements. Mechanical power is measured by means of a torque transducer and an encoder (12).

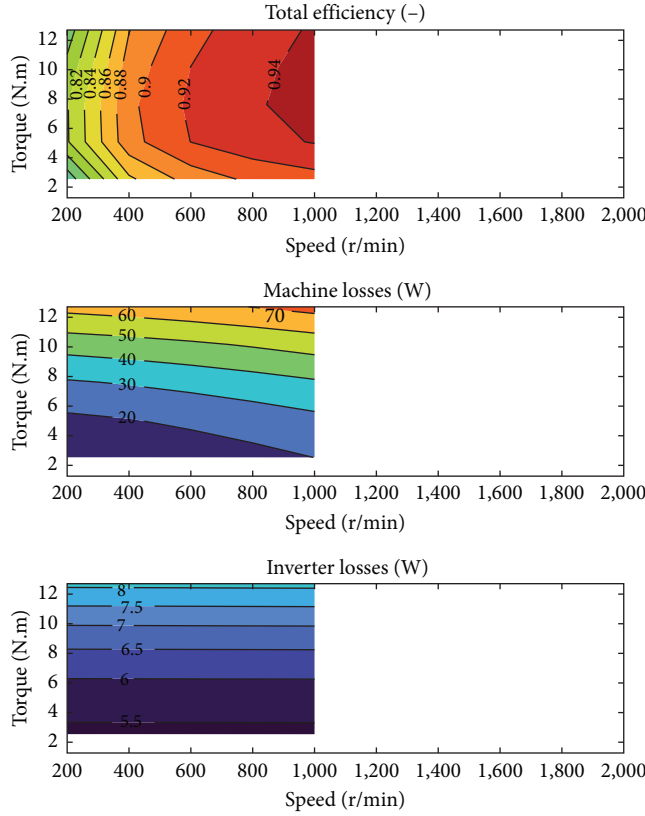


FIGURE 6: Simulated efficiency, machine losses, and inverter losses for the series configuration.

same shaft. The speed of the induction machine is controlled by means of a Siemens SINAMICS drive. A Lorenz DR-2112 torque transducer with a measurement range of $\pm 50 \text{ N}\cdot\text{m}$ and an accuracy of 0.1% is mounted on the shaft between this load motor and the AFPMSM. An incremental encoder with 1,024 pulses per revolution at the side of the induction machine provides a position and a speed measurement. The test setup is equipped with nine LEM LA 25P current transducers (with a nominal RMS current of 25 A and an accuracy of $\pm 0.95\%$) to measure the following three-phase currents: the three-phase current i_{abc} that is applied by the inverter, the three-phase current $i_{abc,1}$ that runs through the first parallel path (i.e., windings A_1 , B_1 , and C_1 in Figure 2), and the three-phase current $i_{abc,2}$ that runs through the second parallel path (i.e., windings A_2 , B_2 , and C_2 in Figure 2). As the sum of each three-phase current set is zero, six LEM modules would have sufficed as well. The maximum current amplitude for the three-phase current i_{abc} equals 9 A. This current limit will be referred to as the inverter's current rating throughout this work. The current amplitude limit for $i_{abc,1}$ and $i_{abc,2}$ is equal to 5 A, and this current limit is called the PMSM's current rating in the remainder of this article. Only the three-phase current i_{abc} provides feedback to the current controller of the AFPMSM, which is implemented on a dSPACE MicroLabBox. The six LEM modules that measure the currents $i_{abc,1}$ and $i_{abc,2}$ are only used for monitoring and could hence be omitted. A Voltech PM6000 Precision Power Analyzer with a bandwidth of 10 MHz and an

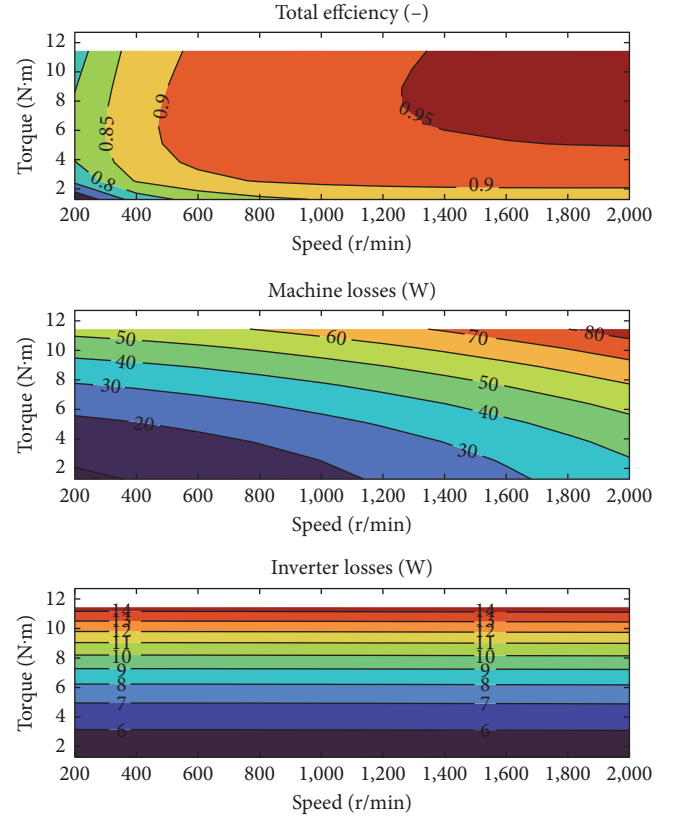


FIGURE 7: Simulated efficiency, machine losses, and inverter losses for the parallel configuration.

accuracy of 0.02% for power loss and efficiency measurements is used to conduct electrical power measurements.

3. Static Behaviour and Operating Range

Switching from the series to the parallel configuration halves the back EMF of the PMSM and hence allows for a doubling of the speed range for the same DC bus voltage. The relation between the torque ranges of the two configurations, however, depends on the inverter's current rating and/or the PMSM's current rating. When the inverter is rated for the series connection (i.e., when the inverter's current rating equals the PMSM's current rating), the parallel configuration can only produce half the torque level of the series connection. This is due to the fact that the inverter current has to split over the two parallel branches. However, when the inverter is rated for the parallel connection, both configurations can achieve the same torque level.

To assess the static behaviour and the operating range of the series and the parallel configuration of the e-gear, it is first studied in simulation. A finite element (FE) model of the AFPMSM (in Comsol) is used to estimate the machine losses (i.e., the copper losses, the core losses [19], and the eddy current losses in the rotor [20]). The iron and magnet losses are computed by means of the multislice 2D approach described in [18, 21]. Skin and proximity effects can be considered as negligible in the thin copper wires and are hence not taken into account in the calculation of the copper losses.

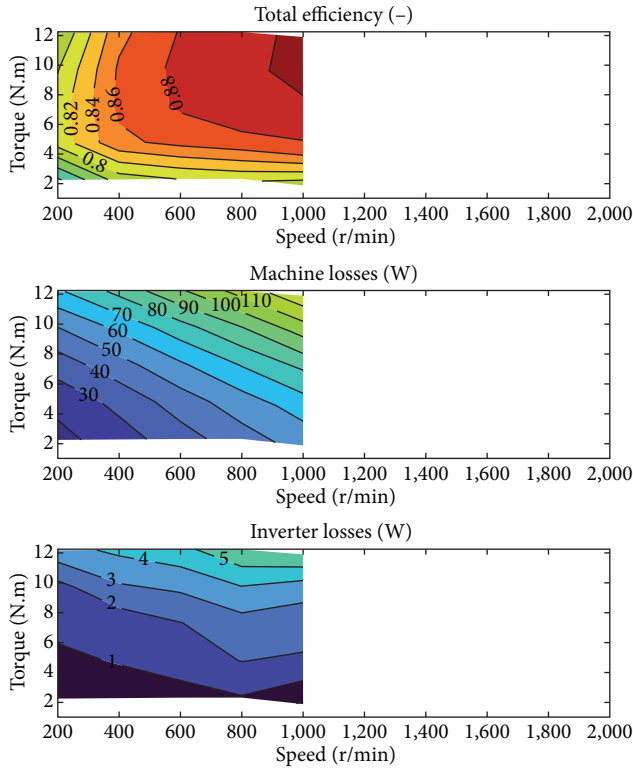


FIGURE 8: Experimentally obtained efficiency, machine losses, and inverter losses for the series configuration.

A MATLAB Simulink/Simscape R2021b simulation model with a variable-step solver with a relative tolerance of 1×10^{-3} is used to estimate the inverter losses and the losses in the reconfiguration unit. This MATLAB simulation model includes the control and reconfiguration strategy, a model of the converter, the reconfiguration unit, and the electrical machine. The AFPMSM is modelled by means of a custom-made Simscape block, based on the six-phase state space model in the abc reference frame that is discussed in Section 4.2. The 2L-VSI and the reconfiguration unit are modelled by means of standard Simscape building blocks. The load motor is not explicitly incorporated in the simulation model: It is assumed that the speed of the AFPMSM is exactly equal to the reference speed at every time instant. The parameters used in the simulation model are obtained from datasheets, the FE model, and measurements. For each simulated operating point, the mechanical relays are continuously steered to establish, respectively, a series or a parallel connection. The AFPMSM and its three-phase inverter are controlled by means of a standard three-phase field-oriented vector current controller, with anti-reset windup and feedforward to decouple the d - and the q -axis. Each configuration has its own set of control parameters. In this work, it is chosen to use the PI parameters $K_p = 11.6$ and $K_i = 4,000$ for both configurations and for both the d - and q -axis. The feedforward terms, however, are different for each configuration. The required machine parameters are listed in Table 1. The sampling and switching frequency is equal to 10 kHz, while the controller's update frequency amounts to 5 kHz.

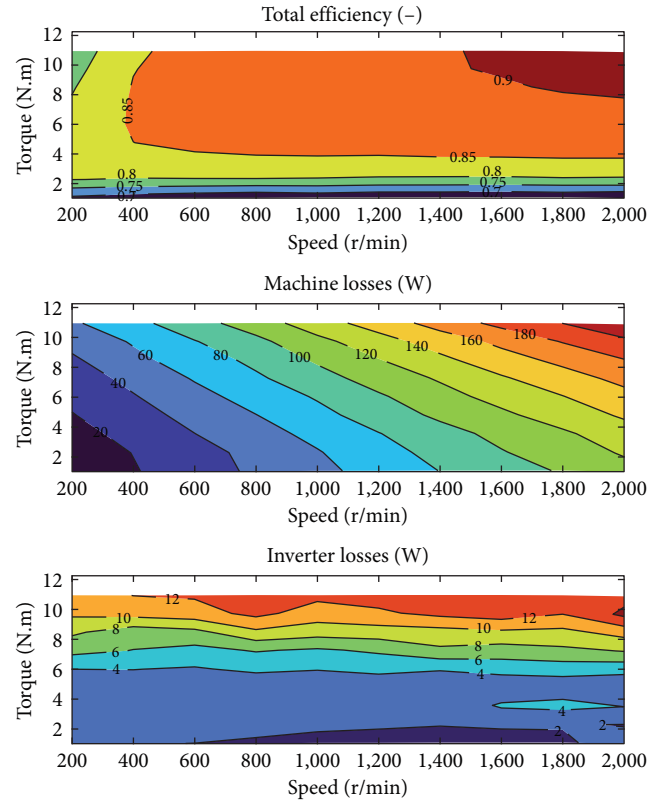


FIGURE 9: Experimentally obtained efficiency, machine losses, and inverter losses for the parallel configuration.

The simulated efficiency map of the complete drive (i.e., AFPMSM, inverter, and reconfiguration switches) is shown in Figure 6 for the series connection, together with the machine losses and the inverter losses. The simulations are performed at mechanical speeds $N = \{200, 400, \dots, 1,000\}$ r/min and q -current set points $I_q^* = \{1, 2, \dots, 5\}$ A. A similar graph is shown in Figure 7 for the parallel connection, with simulation points $N = \{200, 400, \dots, 2,000\}$ r/min and $I_q^* = \{1, 2, \dots, 9\}$ A.

The simulation results of Figures 6 and 7 are experimentally validated on the test setup described in Section 2. The results for the series connection are shown in Figure 8. The results for the parallel connection are presented in Figure 9. The difference between the simulated machine losses and the experimentally obtained machine losses is caused by an underestimation of the core losses in the FE simulation: The degradation of the material properties of the stator core laminations due to the laser cutting process is not taken into account in the FE model but can increase the core losses with 150% [22].

However, in general, the simulations and experiments show the same trends. It can indeed be concluded that switching from a series to a parallel connection allows to double the speed range, that is, from 1,000 to 2,000 r/min for the same DC bus voltage $V_{DC} = 400$ V. For the series connection, the torque range is limited to 12.3 N.m due to the PMSM's current limit of 5 A. In the parallel connection, it is the inverter's current rating of 9 A that limits the current

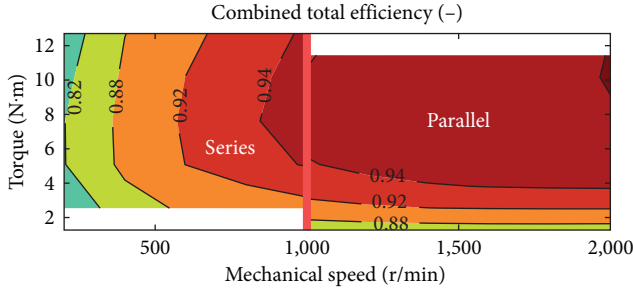


FIGURE 10: Simulated efficiency map for the extended operating range. For mechanical speeds lower than 1,000 r/min, the series configuration is used. For speeds above 1,000 r/min, the parallel configuration is used.

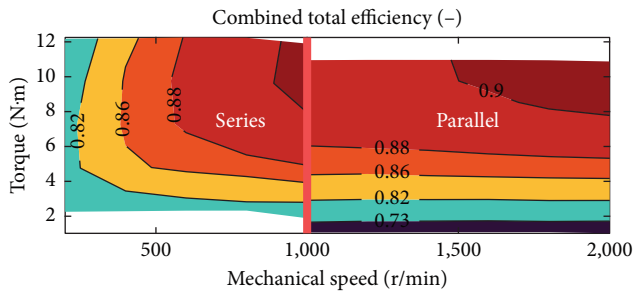


FIGURE 11: Experimentally obtained efficiency map for the extended operating range. For mechanical speeds lower than 1,000 r/min, the series configuration is used. For speeds above 1,000 r/min, the parallel configuration is used.

through the PMSM to 4.5 A and the torque to 11 N·m. The parallel configuration suffers from higher inverter losses than the series configuration for the same torque/speed operating points. This is due to the fact that the inverter has to deliver twice the current to the parallel configuration compared to the series configuration in order to obtain the same torque level. The machine losses are similar for both configurations. In theory, the machine losses are slightly higher for the parallel configuration, since its lower stator inductance introduces more current ripple. However, the mechanical power measurement (based on the sensor inputs of the incremental encoder and the torque transducer) is not accurate enough to observe this phenomenon at all common operating points. The effect on the efficiency of the addition of the six mechanical relays to the original drive is also limited: For the same operating range (i.e., for a torque $T_{em} \in [2 \text{ } 12] \text{ N}\cdot\text{m}$ and a speed $N \in [200 \text{ } 1,000] \text{ r/min}$), the original drive (without reconfiguration unit) exhibits a measured average efficiency of 84.93%, whereas the average efficiency of the e-gear is measured to be 84.84%. This corresponds to an average loss of 7.15 W in the reconfiguration unit. In simulation, the losses in the reconfiguration unit are estimated to be 0.19 W on average.

The joint operating range and efficiency map are shown in Figures 10 (simulation) and 11 (measurement). It confirms that the series/parallel reconfiguration can extend the efficient operating range of a PMSM. For low speeds, the

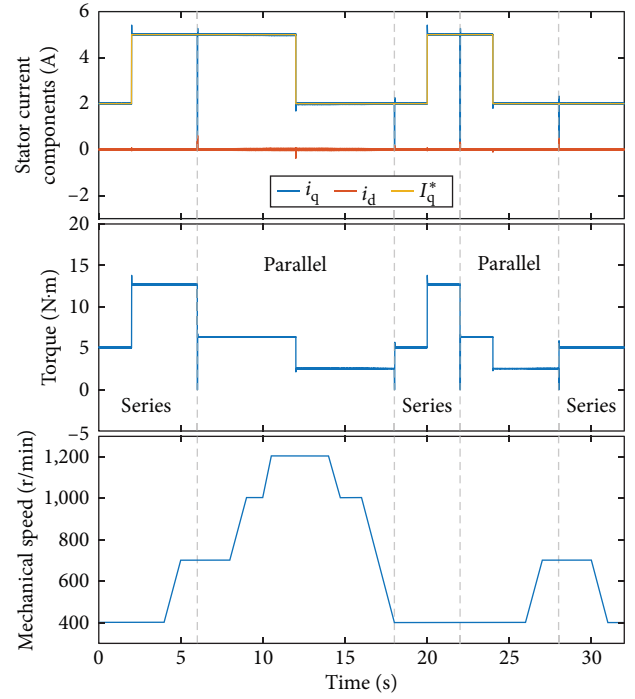


FIGURE 12: Simulation results for the e-gear at different configurations, speeds, and torque levels.

series configuration is used. For high speeds, the parallel configuration is used.

4. Reconfiguration Strategy

4.1. Control Algorithm. To switch from one configuration to the other, the following procedure is followed:

- (1) Open all the switches of the 2L-VSI, in order to block the current in the PMSM and the relays during the reconfiguration. The wear of the mechanical relays is limited in this way. Start resetting the PI controller, and load the new control parameters.
- (2) Wait until the currents that are running through the PMSM and the relays have died out through the anti-parallel diodes.
- (3) Initiate the actual reconfiguration by sending the appropriate steering signals to the mechanical relays.
- (4) Wait until the contacts of the relays are opened or closed again and the bouncing has stopped.
- (5) Stop resetting the PI controller. Resume normal operation with the new control parameters.

4.2. Simulation Results. To simulate the transient response of the PMSM during reconfiguration, the PMSM is modelled as a six-phase machine in the abc reference frame, with windings $A_1, B_1, C_1, A_2, B_2,$ and C_2 as shown in Figure 2:

$$\mathbf{v} = \mathbf{R}\mathbf{i} + \mathbf{L}\frac{d\mathbf{i}}{dt} + \mathbf{e}, \quad (1)$$

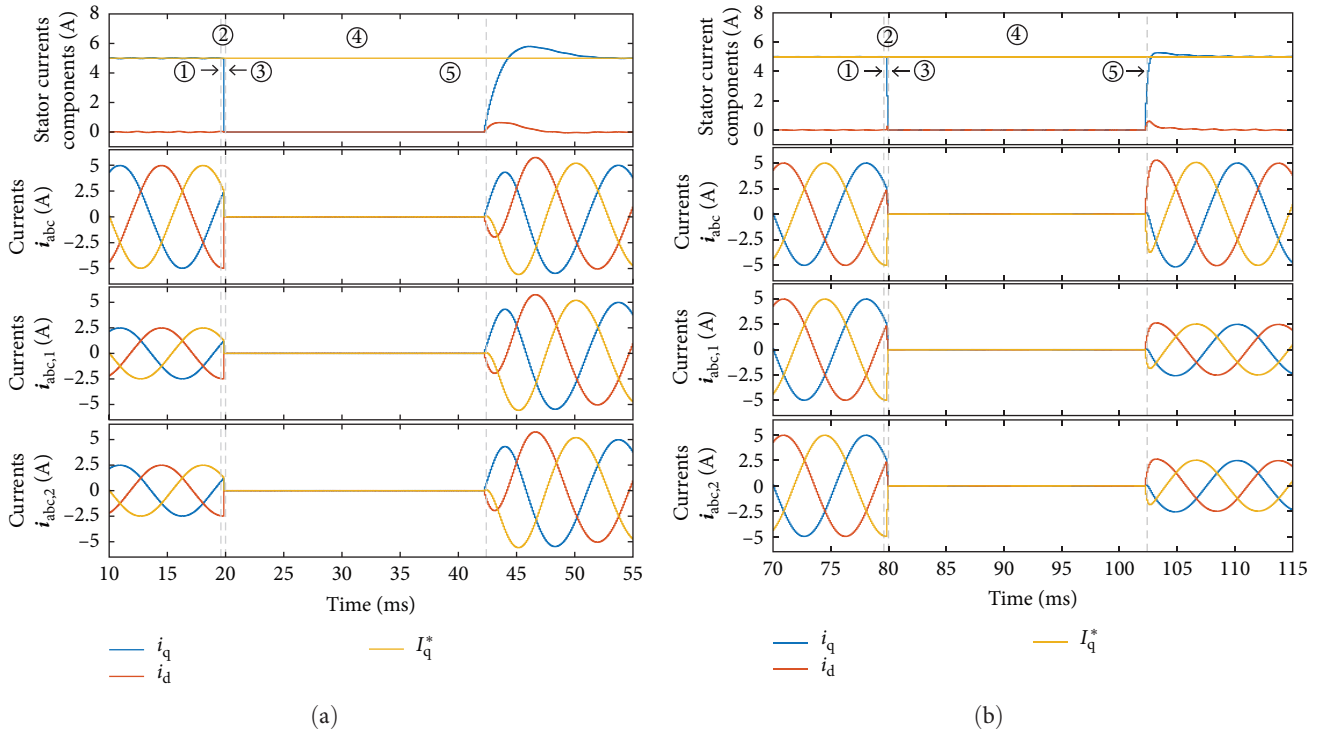


FIGURE 13: Simulated detail of the reconfiguration between parallel and series connection ($I_q^* = 5$ A, $N = 700$ r/min). The five steps of the switching procedure described in Section 4.1 are indicated: (a) reconfiguration from parallel to series and (b) reconfiguration from series to parallel.

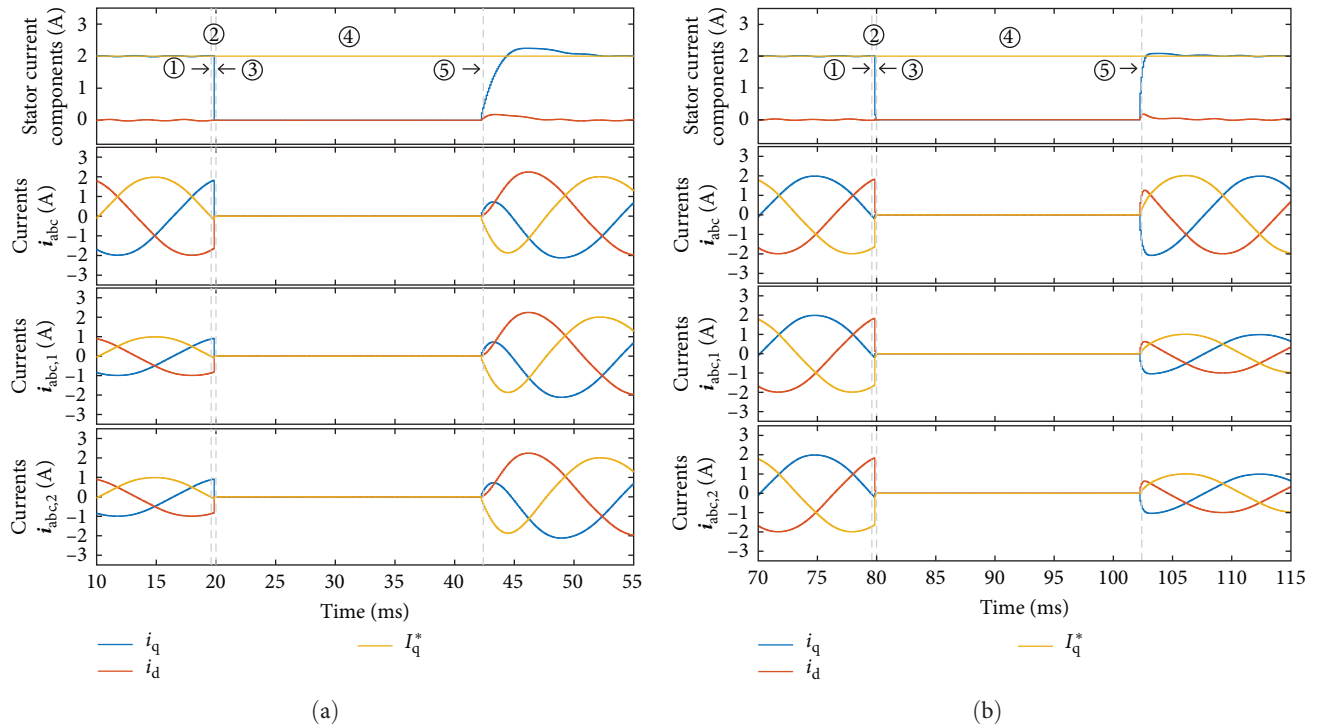


FIGURE 14: Simulated detail of the reconfiguration between parallel and series connection ($I_q^* = 2$ A, $N = 400$ r/min). The five steps of the switching procedure described in Section 4.1 are indicated: (a) reconfiguration from parallel to series and (b) reconfiguration from series to parallel.

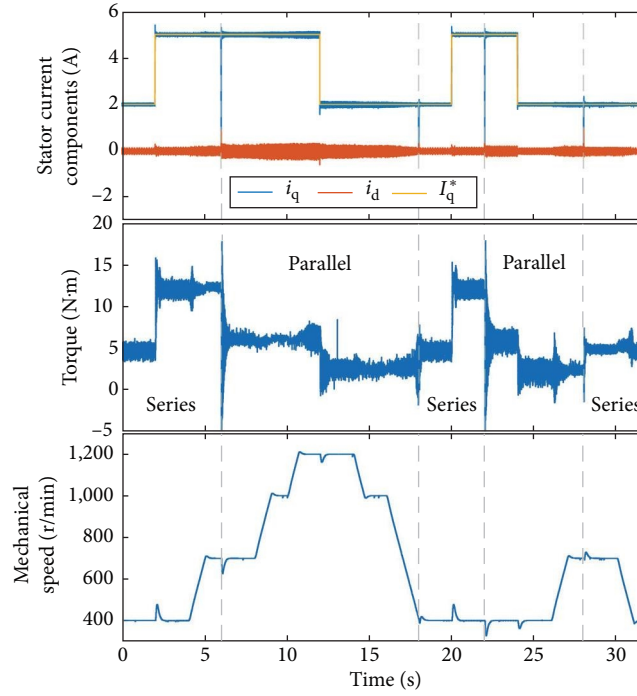


FIGURE 15: Experimental results for the e-gear at different configurations, speeds, and torque levels.

with $\mathbf{x} = [x_{a,1} \ x_{b,1} \ x_{c,1} \ x_{a,2} \ x_{b,2} \ x_{c,2}]^T (\mathbf{x} \in \{\mathbf{v}, \mathbf{i}, \mathbf{e}\})$, $\mathbf{R} = \text{diag}[R_s, \dots, R_s]$, and

$$\mathbf{L} = \begin{bmatrix} L_m & M_1 & M_1 & M_2 & M_3 & M_3 \\ M_1 & L_m & M_1 & M_3 & M_2 & M_3 \\ M_1 & M_1 & L_m & M_3 & M_3 & M_2 \\ M_2 & M_3 & M_3 & L_m & M_1 & M_1 \\ M_3 & M_2 & M_3 & M_1 & L_m & M_1 \\ M_3 & M_3 & M_2 & M_1 & M_1 & L_m \end{bmatrix}. \quad (2)$$

\mathbf{v} represents the stator voltages (V), \mathbf{R} is the stator resistance matrix (Ω), \mathbf{i} represents the stator currents (A), \mathbf{L} is the inductance matrix (H), and \mathbf{e} contains the back EMF caused by the permanent magnets (V). The machine parameters are listed in Table 1.

Figure 12 shows simulation results for different speed and torque levels. The simulation starts in the series connection, after which the winding connection of the AFPMSM is reconfigured at $t \in \{6, 18, 22, 28\}$ s. It can be noticed that the torque level is twice as high for the series connection as for the parallel connection under the same current set point I_q^* . Under the parallel configuration, the speed can be raised above 1,000 r/min, while this is not possible under the series configuration. A detail of the simulated switching transient from parallel to series configuration is presented in Figure 13(a) for the operating point $I_q^* = 5$ A and $N = 700$ r/min. The five reconfiguration steps described in Section 4.1 are indicated on the graph. For $t < 19.6$ ms, the stator windings are connected in a parallel configuration, with the mechanical relays in the positions indicated in Figure 2(b). This means that the three-phase

current \mathbf{i}_{abc} has an amplitude of 5 A, while the current amplitude of $\mathbf{i}_{abc,1}$ and $\mathbf{i}_{abc,2}$ through the parallel branches equals 2.5 A. The three 3-phase current sets are in phase with each other. At $t = 19.6$ ms, the current through the PMSM and the relays are interrupted by opening all the switches of the 2L-VSI. Only four switching periods later (at $t = 20$ ms), when the currents have died out, the relays are switched from their positions in Figure 2(b) to their positions in Figure 2(a). For the Potter & Brumfield T9GS5L14-5 mechanical relays used in this work, the maximum operate or release time including bounce equals 22 ms. The normal operation of the drive in series connection is hence resumed at $t = 42$ ms, with the control parameters for the series connection. After the control transients have died out, a current with an amplitude of 5 A runs through all the windings of the PMSM. The switching transients hence take less than 35 ms, making the e-gear competitive with the gearbox of a Lamborghini Aventador, which has a reported shift time of 50 ms [10].

Figure 13(b) shows a zoomed in view of the simulated reconfiguration from a series to a parallel connection. The current is interrupted at $t = 79.6$ ms, after which the switching of the mechanical relays is started at $t = 80$ ms. The operation of the PMSM in parallel connection is resumed 22 ms later.

For completeness, Figure 14 presents the transients for another operating point as well (i.e., $I_q^* = 2$ A and $N = 400$ r/min). Also at this operating point, the reconfiguration transients have died out after 35 ms.

4.3. Experimental Validation. Experimental results obtained with the test setup of Figure 5 are shown in Figure 15 for different speeds and torque levels. As in the simulation of Figure 12, the experiment starts in the series connection, after which the winding connection of the AFPMSM is reconfigured

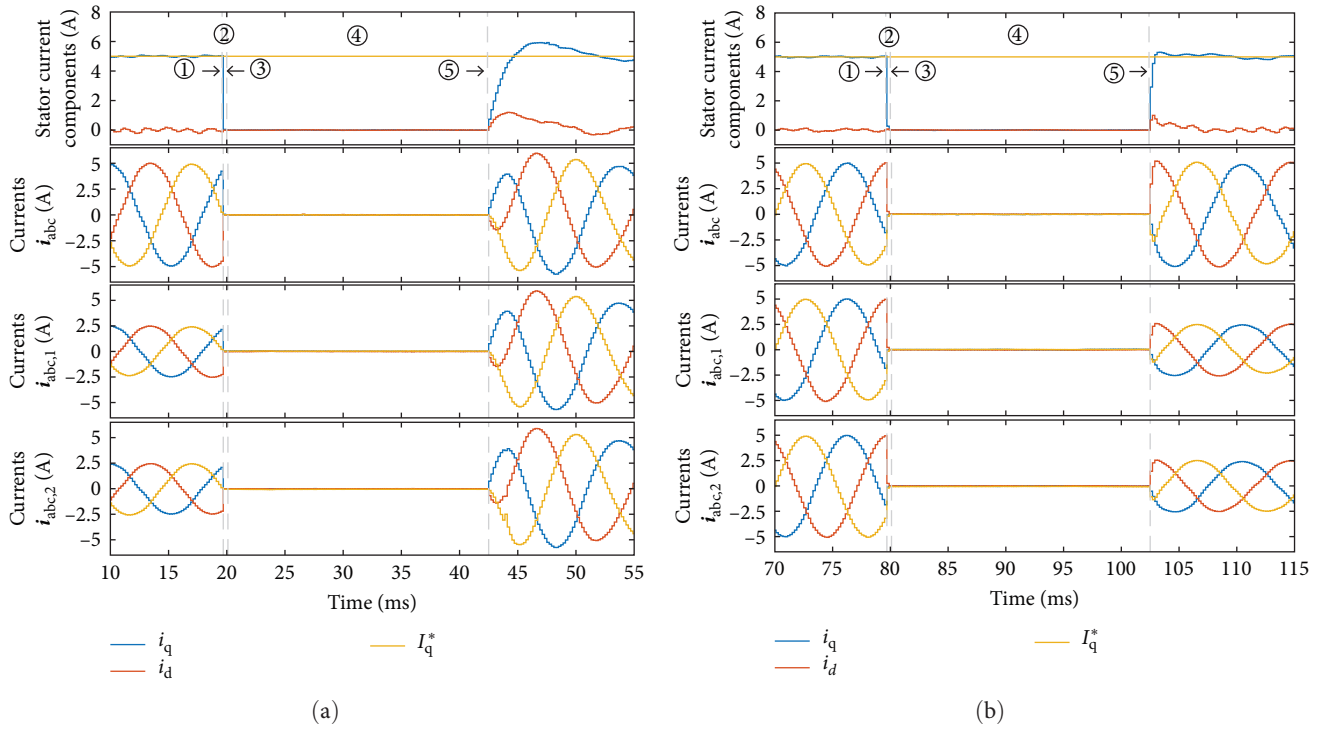


FIGURE 16: Measured detail of the reconfiguration between parallel and series connection ($I_q^* = 5$ A, $N = 700$ r/min). The five steps of the switching procedure described in Section 4.1 are indicated: (a) reconfiguration from parallel to series and (b) reconfiguration from series to parallel.

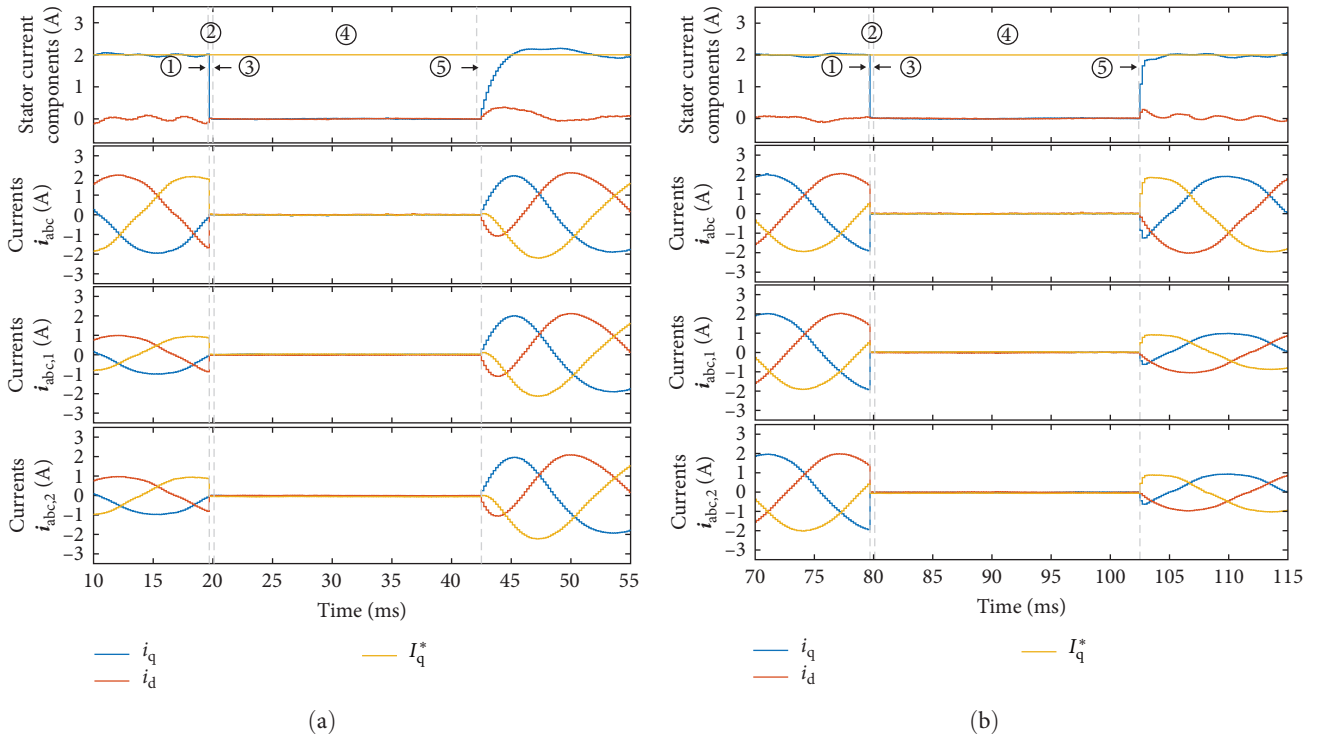


FIGURE 17: Measured detail of the reconfiguration between parallel and series connection ($I_q^* = 2$ A, $N = 400$ r/min). The five steps of the switching procedure described in Section 4.1 are indicated: (a) reconfiguration from parallel to series and (b) reconfiguration from series to parallel.

at $t \in \{6, 18, 22, 28\}$ s. Apart from the measurement noise on the torque signal and the fact that the load motor is not able to keep the speed perfectly constant under a torque variation, the experimental results of Figure 15 are in good agreement with the simulation results of Figure 12. In the parallel configuration, the speed can indeed be raised above 1,000 r/min. For the same q -current set point I_q^* , the torque level is indeed twice as high for the series configuration as for the parallel configuration.

Details of the reconfiguration transients are shown in Figures 16 and 17 for the same operating conditions as in simulation (i.e., $I_q^* = 5$ A and $N = 700$ r/min and $I_q^* = 2$ A and $N = 400$ r/min, respectively). The experiments are in good agreement with the simulation results of Figures 13 and 14. They both confirm that the reconfiguration transients fade away in less than 35 ms. The e-gear thus indeed outperforms the shift time of the gearbox of a Lamborghini Aventador.

5. Conclusion

This work presents an e-gear that allows to change the winding connections of a PMSM from a series connection to a parallel connection and vice versa while the machine is running. The series connection makes it possible to achieve the maximum torque level, while the parallel connection doubles the efficient speed range of the drive. The e-gear can be established by retrofitting a standard three-phase PMSM fed by a standard three-phase 2L-VSI with a switching unit comprising six mechanical relays. The only requirements for the PMSM are that it has open-end windings and that it has two paths per phase with identical back EMF. These parallel paths can be created by means of a bifilar winding. During the reconfiguration, the current through the machine and the relays is blocked, in order to limit the wear of the mechanical relays. Both simulations and measurements on a 4-kW test setup validated the reconfiguration strategy. They confirm that the switching unit has almost no impact on the efficiency of the drive and that all the reconfiguration transients have died out after less than 35 ms. The shift time of the e-gear is hence competitive with the shift time of the most advanced mechanical gearboxes in cars.

In future work, the e-gear must be tested in a realistic driving cycle in order to assess its performance as part of an electric vehicle.

Data Availability

The data that support the findings of this study are available from the corresponding author upon reasonable request.

Conflicts of Interest

The authors have declared no conflict of interest.

Acknowledgments

This work was supported by the Research Foundation-Flanders (FWO). L. Verkrust was awarded a PhD fellowship strategic basic research from the FWO in 2019 (project number 3S045319). This project has received funding from the European Union's Horizon Europe Research and Innovation

Program under grant agreement no 101056824. Views and opinions expressed are however those of the authors only and do not necessarily reflect those of the European Union or CINEA. Neither the European Union nor CINEA can be held responsible for them.

References

- [1] I. Husain, B. Ozpineci, M. S. Islam et al., "Electric drive technology trends, challenges, and opportunities for future electric vehicles," *Proceedings of the IEEE*, vol. 109, no. 6, pp. 1039–1059, 2021.
- [2] Z. Wang, T. W. Ching, S. Huang, H. Wang, and T. Xu, "Challenges faced by electric vehicle motors and their solutions," *IEEE Access*, vol. 9, pp. 5228–5249, 2021.
- [3] M. M. Swamy, T. Kume, A. Maemura, and S. Morimoto, "Extended high-speed operation via electronic winding-change method for AC motors," *IEEE Transactions on Industry Applications*, vol. 42, no. 3, pp. 742–752, 2006.
- [4] T. Deng, Z. Su, J. Li, P. Tang, X. Chen, and P. Liu, "Advanced angle field weakening control strategy of permanent magnet synchronous motor," *IEEE Transactions on Vehicular Technology*, vol. 68, no. 4, pp. 3424–3435, 2019.
- [5] T. Senjyu, Y. Noguchi, N. Urasaki, A. Yona, H. Sekine, and T. Funabashi, "Wide-speed-range optimal PAM control for permanent magnet synchronous motors," in *2007 7th International Conference on Power Electronics*, pp. 916–921, IEEE, Daegu, Korea (South), October 2007.
- [6] Y. Matsumura and N. Urasaki, "Comparison between PAM control and flux weakening control for PMSM drive," in *2012 15th International Conference on Electrical Machines and Systems (ICEMS)*, pp. 1–5, IEEE, Sapporo, Japan, October 2012.
- [7] Y.-S. Lin, K.-W. Hu, T.-H. Yeh, and C.-M. Liaw, "An electric-vehicle IPMSM drive with interleaved front-end DC/DC converter," *IEEE Transactions on Vehicular Technology*, vol. 65, no. 6, pp. 4493–4504, 2016.
- [8] "Variable coil configuration system control, apparatus and method," U.S. Patent US 2020/0 076 345 A1, Mar. 5, 2020.
- [9] H. Xia, Y. Zhang, D. Zhou et al., "Impact of loss model selection on power semiconductor lifetime prediction in electric vehicles," in *IECON 2022—48th Annual Conference of the IEEE Industrial Electronics Society*, pp. 1–7, IEEE, Brussels, Belgium, October 2022.
- [10] V. Radu, "The Aventador's ISR gearbox: how it works and why some owners complain about it," 2021, accessed Dec. 31, 2023, <https://www.autoevolution.com/news/the-aventador-s-isr-gearbox-how-it-works-and-why-some-owners-complain-about-it-164507.html>.
- [11] TE Connectivity, "Relay contact life," 2023, accessed Dec. 14, https://www.te.com/commerce/DocumentDelivery/DDEController?Action=srchrtv&DocNm=13C3236_AppNote&DocType=CS&DocLang=EN#:~:text=The%20electrical%20life%20expectancy%20of,or%20even%20100%20million%20operations.
- [12] "Inverter driving method for induction motors," U.S. Patent 4 916 376, 1990.
- [13] S. Sadeghi, L. Guo, H. A. Toliyat, and L. Parsa, "Wide operational speed range of five-phase permanent magnet machines by using different stator winding configurations," *IEEE Transactions on Industrial Electronics*, vol. 59, no. 6, pp. 2621–2631, 2012.
- [14] T. Kume, T. Iwakane, T. Sawa, T. Yoshida, and I. Nagai, "A wide constant power range vector-controlled AC motor drive

- using winding changeover technique," *IEEE Transactions on Industry Applications*, vol. 27, no. 5, pp. 934–939, 1991.
- [15] Y. Takatsuka, H. Hara, K. Yamada, A. Maemura, and T. Kume, "A wide speed range high efficiency EV drive system using winding changeover technique and SiC devices," in *2014 International Power Electronics Conference (IPEC-Hiroshima 2014—ECCE ASIA)*, pp. 1898–1903, IEEE, Hiroshima, Japan, May 2014.
- [16] Y. Shin, S. Cho, H. Jung et al., "A thyristor-based seamless winding changeover circuit for high efficiency of electric vehicle drive system," in *2019 10th International Conference on Power Electronics and ECCE Asia (ICPE. 2019—ECCE Asia)*, pp. 1274–1279, IEEE, Busan, Korea (South), May 2019.
- [17] S.-H. Im and B.-G. Gu, "A snubberless solid-state tap changer for permanent magnet synchronous motors," *IEEE Transactions on Power Electronics*, vol. 35, no. 11, pp. 12143–12152, 2020.
- [18] H. Vansompel, "Design of an energy efficient axial flux permanent magnet machine," Ph.D. dissertation, Ghent University, 2013.
- [19] D. Kowal, P. Sergeant, L. Dupré, and A. Van den Bossche, "Comparison of nonoriented and grain-oriented material in an axial flux permanent-magnet machine," *IEEE Transactions on Magnetics*, vol. 46, no. 2, pp. 279–285, 2010.
- [20] H. Vansompel, P. Sergeant, and L. Dupre, "A multilayer 2-D–2-D coupled model for eddy current calculation in the rotor of an axial-flux PM machine," *IEEE Transactions on Energy Conversion*, vol. 27, no. 3, pp. 784–791, 2012.
- [21] P. Sergeant, H. Vansompel, A. Hemeida, A. Van den Bossche, and L. Dupre, "A computationally efficient method to determine iron and magnet losses in VSI-PWM fed axial flux permanent magnet synchronous machines," *IEEE Transactions on Magnetics*, vol. 50, no. 8, pp. 1–10, 2014.
- [22] R. Sundaria, A. Hemeida, A. Arkkio, A. Daem, P. Sergeant, and A. Belahcen, "Effect of different cutting techniques on magnetic properties of grain oriented steel sheets and axial flux machines," in *IECON. 2019—45th Annual Conference of the IEEE Industrial Electronics Society*, pp. 1022–1027, IEEE, Lisbon, Portugal, October 2019.